Bull. Mater. Sci. (2018) 41:11
https://doi.org/10.1007/s12034-017-1524-8

© Indian Academy of Sciences

Role of surface thermal properties of HfB_2 nanoparticles on heat flow in MWCNT/novolac composites

ZAHRA AMIRSARDARI[1], ROUHOLLAH MEHDINAVAZ AGHDAM[2,*] and MOHAMMAD REZA JAHANNAMA[1]

[1]Space Transportation Research Institute, Iranian Space Research Center, Tehran, Iran
[2]School of Metallurgy and Materials Engineering, College of Engineering, University of Tehran, Tehran 1417466191, Iran
*Author for correspondence (mehdinavaz@ut.ac.ir)

MS received 6 August 2016; accepted 10 July 2017; published online 2 February 2018

Abstract. Carbon–novolac composites (C–C) modified by HfB_2 and MWCNT were ablated by an oxyacetylene torch at 2500°C to investigate the thermal behaviour and the mechanism of mass loss of the samples. Two phenolic matrix composites containing 4 wt% HfB_2 nanoparticle and with or without MWCNT were fabricated. These nanoparticles dissipate heat throughout the sample, thereby reducing thermal gradients, reducing the intensity of heating at the surface exposed to flame, and insulating the carbonaceous char with the network of HfO_2/MWCNT/char. During ablation, HfO_2 particles formed and functioned as a thermal barrier, and MWCNT char phase acted as an oxygen diffusion barrier, protecting composites from further ablation.

Keywords. Hafnium diboride nanoparticles; multi-walled carbon nanotube; phenolic composites; thermal management.

1. Introduction

Carbon–carbon composites are a family of materials that possess extraordinary and unique characteristics that make them attractive for use in a wide range of applications, especially when low-density materials are desirable, such as in aerospace applications [1]. Phenolic resins are indeed irreplaceable materials for many specific high-technology applications such as thermal-protection systems. High-char yield, good thermal stability, low-smoke producing on burning and low flammability are the characteristics that make phenolic resins attractive candidates for various applications. Since phenolic resins are aromatic compounds with one or more hydroxyl groups attached to an aromatic ring—they typically exhibit good heat resistance—are rather flame-resistant, and have good dimensional stability for ablative heat shields [2]. One of the most serious drawbacks of the phenolic composites is their oxidation sensitivity at a temperature as low as 500°C in oxidizing environmental conditions as high-temperature structural composites [3]. Therefore, it is essential to enhance the ability of oxidation and ablation resistance from the rigorous heating effects confronted in high-temperature operation. Also, to reduce the erosion phenomena of carbon nanotube/phenolic ablators, several kinds of improved phenolic composites were evaluated. Accordingly, the best way is the addition of another filler to improve thermal properties in phenolic composites. Ultra-high temperature ceramics (UHTCs), particularly diborides and carbides of the transition metals such as hafnium are currently accepted as potential candidates for a variety of thermal applications [4]. Hafnium diboride (HfB_2) has lower melting point (3100°C) than hafnium carbide (3890°C), but the measurement confirmed that the level of thermal conductivity of HfB_2 is higher than HfC. Its higher value improves a material's thermal-shock resistance by reducing temperature gradients and thermal stresses within the material. It also allows more energy to be conducted away from the stagnation point and spreading the heat over a larger component surface area [5]. More recently, a number of researchers have focussed on introducing HfC compounds into C–C composites [6–10]. But very few research studies involving ablation and thermal process of HfB_2 in carbon composites were conducted so far. Paul *et al* [11] reported the preparation of hafnium diboride particles (<44 μm) in carbon fibre/phenolic composites to improve the high-temperature oxidation resistance. Li *et al* [2] modified the thermal properties of carbon–carbon composites by hafnium diboride using a two-step process of *in situ* reaction and thermal gradient chemical vapour infiltration. Ren *et al* [12] reported the preparation of HfB_2–SiC coating for SiC-coated C–C composites by *in situ* reaction method for blocking the penetration of oxygen and providing an effective protection for the C–C substrate. The present investigation, for the first time, details the use of hafnium diboride particles in the nanoscale size (∼50 nm) in carbon–phenolic to the increment of thermal resistance through the system, especially in the boundary layer. The use of HfB_2 nanoparticles as an ablative material to obtain low-thermal conductive thermal protection system (TPS) is an innovative idea. Oxidation at high temperatures produces a layered oxide scale in the outer

layer and the non-oxidized bulk [13]. Furthermore, polymer composites were tested with wide range reinforcements to assist char retention. In recent advances, studies were focussed on the development of HfB_2 reinforced with SiC, because of their remarkably better thermal stability than common composite materials [14]. In this work, SiC substituted by multi-walled carbon nanotube (MWCNT) and incorporated into a polymeric phenolic network through a facile route to synthesize a novel nanocomposite. Thermal properties of this nanocomposite make it an effective candidate as an ablative system for heat shields.

Research studies explain the influence of the incorporation of ceramic in the polymer matrix on thermal properties [15–17], and the effect of the addition of MWCNT and graphene on ablative and flame-retarding properties of the phenolic composite are available [18–21]. Extensive research on various modified phenolic matrices was done to achieve better ablative properties, but till now, HfB_2 nanoparticles in the novolac composites were never prepared, studied and tested by any research group for its ablation rates or for its application in the TPS that was employed as a heat shield.

The main objectives of the present study are to focus on (i) preparation of novel HfB_2 nanoparticles/carbon–novolac resin and its comparison with novolac composite, and modification of novel HfB_2/novolac resin by adding 1 wt% of MWCNT, which was explained by the enhancement of char retention property; (ii) effectiveness of the modified composite as a mechanical reinforcing filler; (iii) thermogravimetric (TG) analysis to determine decomposition behaviour and cost-effective oxyacetylene flame test to quantify ablative characteristics and to examine the high-end applicability of the reinforced composite; and (iv) investigation of the effect of addition of these two nanostructures on the integrity and insulating nature of the char network, thermal and surface barrier properties.

2. Experimental

2.1 *Materials*

Novolac resin (containing 5.5–6.5% hexamine, Resitan), carbon fibre (diameter of about 7 μm, Uvicom) and MWCNT (filament diameter 8–15 nm, filament length 50 μm, Neutrino) were used to make phenolic composites. For the HfB_2 nanoparticle synthesis (50 nm), commercial powder of $HfCl_4$, acetylacetone (Aldrich), deionized water, boric acid, citric acid, acetic acid and methanol (Merck) were selected.

2.2 *Nanoparticles preparation*

Initially, 0.006 mol acetylacetone complexing agent was added to 0.0203 mol $HfCl_4$ in 10 ml of methanol and 2 ml of water, and stirred until a homogeneous phase was obtained. Then boric acid and citric acid were slowly added to acetic acid at 80°C, and stirred till the dissolution is complete. These two mixtures were added together, mixed well, and kept at 60°C for 3 h. Citric acid was added to the precursor solution to promote the chelating reaction between metallic cations and carboxylic groups. The boron to hafnium ratio (B/Hf) was set to 4:1, and the carbon to hafnium ratio (C/Hf) was kept at 5:1. The final mixture was transferred into an oven and maintained at 120°C for 2 h, resulting in a dried gel-citrate precursor. Then, the dried powders were calcined to 1500°C with a constant heating rate of 2°C min^{-1}. Finally, nanopowdered HfB_2 with an average particle size of 50 nm was synthesized by a chemical reaction of $HfCl_4$ with H_3BO_3 performed during 2 h at 1500°C in a tubular furnace (Azar Furnace, Iran) sealed under argon atmosphere.

2.3 *Nanocomposite preparation*

For preparation of nanocomposites, weighed quantities of fine HfB_2 (4 wt%) and MWCNT (1 wt%) were mixed in ethanol thoroughly using an ultrasound for 1 h in an ice bath. Subsequently, resin dissolved in ethanol was added, and then sonicated again. The manufacturing process comprised mixing of these ingredients, followed by the addition of carbon fibres (at a weight ratio to the phenolic of 1:1) under mechanical mixing for 2 h to fabricate HfB_2/MWCNT/carbon fibres—novolac mixture. The resulting compounds were placed in an oven at 70°C for 3 h to get rid of the solvent and moisture. The dried mixture was then loaded in a stainless mould frame and hot-pressed at 170°C under a pressure of 10 MPa for 2 h. Finally, to obtain the samples with well-defined shapes, the composites were cut into a size of 25 mm in diameter and 20 mm in height. Three types of composites were fabricated by this procedure are listed in table 1.

2.4 *Nanocomposite characterization*

The hardness (shore D) was studied with hardness testing machine (Zwick 3100) according to ASTM D-2240. The wear tests were carried out on a universal wear tester with pin-on-disc configuration at an applied load of 90 N and the sliding distance corresponding to the surface force interaction between the pin and a tested sample of 300 m. The specimen contact area against the wear test was 3 cm diameter and its thickness was 1 cm. The changes of density and open porosity of composites were also measured using Archimedes' principle. The ablation test was carried out in oxyacetylene torch with heat fluxes of 6 MW m^{-2} at Malek Ashtar University, Tehran, Iran. The inner diameter of the oxyacetylene gun tip was 0.2 cm, and the distance between the gun tip and the composite was 5 cm. Ablation time was controlled at 160 s and the size of the composites was further reduced to 2.5 cm in diameter and 2 cm in length. After ablation, the phase analysis of composite surfaces was conducted by X-ray diffraction (XRD, GNR Co., Explorer). The thermal decomposition behaviour of composites was examined by means of TG (Linseys STA 1600) in nitrogen with a heating rate

Table 1. Properties of novolac composites.

Materials	Composite	Porosity (%)	Density (kg m^{-3})	Hardness (shore D)	Wear rate (10^{-6} mm^3 N^{-1} m^{-1})
Carbon–novolac	C–C	4.69	1.37	49	2.97
HfB_2/carbon–novolac	HB/C–C	3.07	1.34	65	2.12
MWCNT/HfB_2/carbon–novolac	HB/NT/C–C	6.01	1.31	80	0.34

of 10°C min^{-1}. Morphologies and chemical compositions of the prepared and ablated composites were investigated by field emission scanning electron microscope (FESEM, Mira II Tescan) equipped with energy dispersive spectroscopy (EDS). Also, the size of HfB_2 nanoparticles was determined by transmission electron microscope (TEM, Philips CM30).

3. Results and discussion

3.1 *Properties of HfB_2 nanoparticles*

The phase purity and particle size of HfB_2 are influenced by the acid concentration during the gelling and calcination processes. In this way, the citrate precursor method was used to fine-control the cation stoichiometry and the particle size. The advantage of citric acid in a process was that it enhances the mixing of ions at the atomic scale [22]. The process involved is complexation of hafnium ions by poly-functional carboxyl acids (citric acid) with one hydroxyl group. The intermediates that resulted from the reaction of hafnium (IV) ions with acidic solution led to the homogeneous nucleation of HfO_2 seeds. On the other hand, on heating, boric acid converted to B_2O_3 by releasing water. Carbon, which is well distributed between the particles, reacted with oxide species (HfO_2 and B_2O_3) according to equation (1) [23].

$$HfO_2 + B_2O_3 + 5C = HfB_2 + 5CO. \quad (1)$$

Prolonged high temperature elevation (2°C min^{-1}) during carbothermal reduction has promoted precursor evaporation and yielded homogeneous nanostructured powders.

The results extracted from the characterization of HfB_2 are shown in figure 1. The TEM and FESEM images of HfB_2 are shown in figure 1a and b, respectively. The XRD pattern of HfB_2 nanoparticles is indexed in figure 1c as a pure hexagonal structure with the literature value (JCPDS card no. 75-1049). As apparent from the inset of these images, nanoparticles ranged in size between 40 and 60 nm with an average particle size of 50 nm. Local chemical analyses were performed by EDS (figure 1d), simultaneously to the FESEM observations. An EDS spectrum of HfB_2 nanostructure of locations marked in figure 1b calcined at 1500°C showed that only Hf and B were the elemental components, in addition to Au, which came from the FESEM coating process, implying no other impurity in the fabricated sample.

3.2 *Wear and hardness of phenolic nanocomposites*

Table 1 lists the tested wear and hardness for three kinds of carbon fibre-reinforced phenolic composites as well as density and open porosity. It can be seen that HB/NT/C–C has the highest hardness ~80, which is about 1.63 times of C–C. The phenolic composite with HfB_2 show higher hardness than C–C, increased by over 33%. The impregnated nanostructures have efficiently reduced the flow-ability or chain mobility of the novolac matrix that eventually enhanced the hardness of the final sample that may be attributed to the impregnated high hardness [24]. The presence of obstacles to the motion of shear bands are the reasons for the enhancement of hardness in the polymer composites [25]. Also, the wear rates of the composites mixed with nanostructures were smaller than that of the composite without any filler since the wear mechanism was different. Firstly, the wear debris on the C–C composite was formed due to the microcracks and delamination in the matrix. Then, the carbon fibres are broken due to the buckling and delamination from the brittle phenolic matrix. The broken carbon fibres work as abrasive particles on the surface of novolac matrix. In the HB/C–C composite, HfB_2 nanoparticles prevented the catastrophic failure of the brittle phenolic matrix by detouring fatigue cracks [26]. Therefore, the composite with HfB_2 showed a lower wear rate than the composite without these nanoparticles. When both nanostructures were mixed with the C–C composite, the wear rate was lower compared with the composite of HfB_2. The wear rates of the composite with HfB_2 and the composite without any filler were 2.12 and 2.97, respectively, whereas that of the composite with HfB_2 and MWCNT was 0.34. The increase of the hardness and wear resistances by MWCNT addition might be due to the superior mechanical properties of MWCNTs. The small wear rate of the composite with both nanostructures was caused by the resin-rich area of phenolic resin and MWCNT.

The values of density calculated by Archimedes method were nearly the same for three composites. The open pore volume (the percentage porosity) was found to increase a little by adding HfB_2 and MWCNT. The increased pore volume could be explained by the fact that initially during hot-press, the matrix still contains some solvent, which is gradually removed leading to the contraction of the composite resulting in a net reduction of the pore volume. The MWCNT-containing polymer cannot contract as more solvent is removed, holding the structure open and resulting in a larger pore volume.

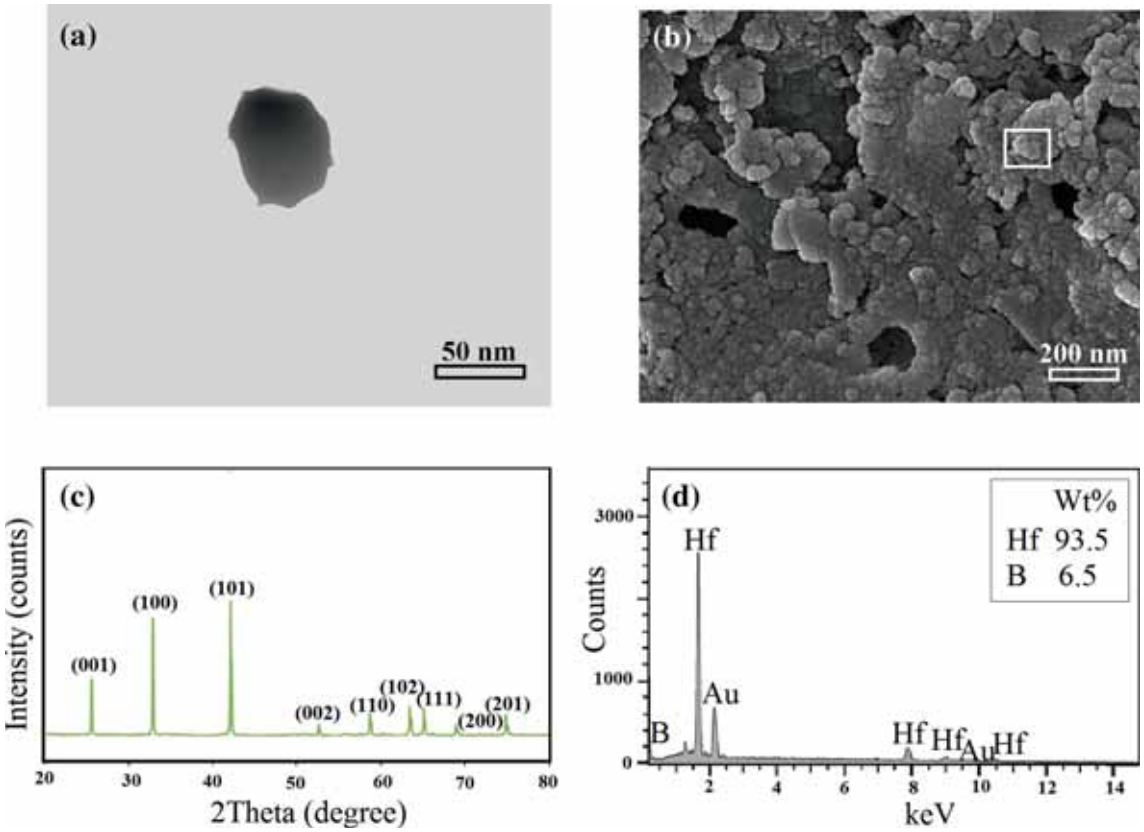

Figure 1. (**a**) TEM, (**b**) FESEM images, (**c**) XRD pattern and (**d**) EDS of HfB_2 nanoparticles synthesized at 1500°C for 2 h.

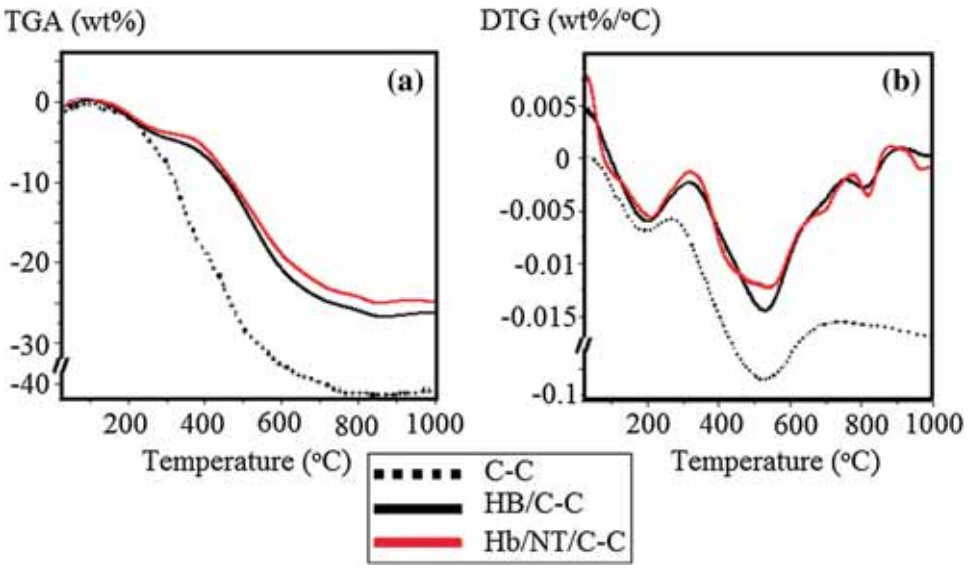

Figure 2. (**a**) TGA and (**b**) DTGA thermograms of original and modified composites under nitrogen atmosphere.

3.3 *Thermal property of the nanocomposites*

During thermogravimetric analysis (TGA) under neutral environment (nitrogen) for the temperature range of 25–1000°C, when the temperature was below 250°C, the weight loss of all the samples was very low, which can be attributed to the loss of residual water in the material, and further the condensation of phenolic matrices. The mass loss

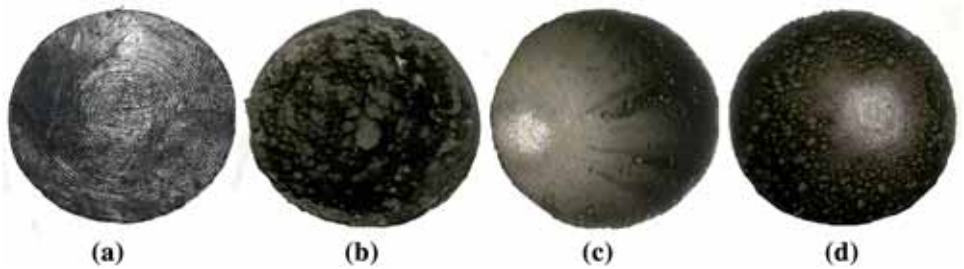

Figure 3. Surface images of (**a**) all three composites before oxyacetylene torch test; and (**b**) C–C, (**c**) HB/C–C and (**d**) HB/NT/C–C after exposure to the flame at 2500°C for 160 s.

curve as a function of temperature (figure 2) of the unmodified carbon–phenolic showed two thermal degradation transitions: (a) the adsorbed water, which volatilizes at low temperatures, and (b) degradation of matrix at higher temperatures. Three mass loss regions were distinguished in the carbon–phenolic nanocomposites: (i) the evolution of water and gaseous species physically adsorbed (below 150°C); (ii) the decomposition of phenolic matrix (between 150 and 600°C); and (iii) the decomposition of HfB_2 nanoparticles (above 800°C). The materials suffered from a major weight loss in the temperature range of 300–650°C. The weight loss around 450–550°C was due to decomposition of phenolic resin, and other weight loss around 600–650°C was due to degradation of carbon fibres in the composites [27]. During this stage, the degradation of terminal hydroxyl and the pyrolysis of the free radical led to the production of small molecule products such as CH_4, CO, CH_2O, C_6H_6 and phenol [28]. The loss was ∼43.32 wt% in the case of unmodified C–C, and 26.97 wt% for HB/C–C composite. The 24.93 wt% of the total mass loss was obtained in the C–C composites with HfB_2 and MWCNT.

3.4 *Properties of HfB_2 nanoparticles*

The oxyacetylene torch test was used to simulate the severe temperature environment. Phenolic resins are an ablative matrix due to its ability to form a char layer on the surface at high temperature [29]. Carbon fibre is usually utilized as a reinforcement in the phenolic resins for the ablation purpose owing to its high carbon content, excellent thermal stability, low thermal expansion and high thermal conductivity [30]. The ablation resistance of the neat composite is weak due to the pyrolysis gases, which makes the char layer peeled off by the high-speed incoming shear heat flux [31]. After ablating by an oxyacetylene torch test at 2500°C for 160 s, the surface morphology and XRD analysis of the composites are shown in figures 3 and 4, respectively. The smoothest surfaces for all the composites were obtained before the test— figure 3a. Figure 4a shows the amorphous carbon system with two broad maxima at 2θ angles of 24 and 44° [32] corresponding to the structures shown in figure 3b. As illustrated in figure 3c and d, the surfaces of HB/C–C and HB/NT/C–C composites

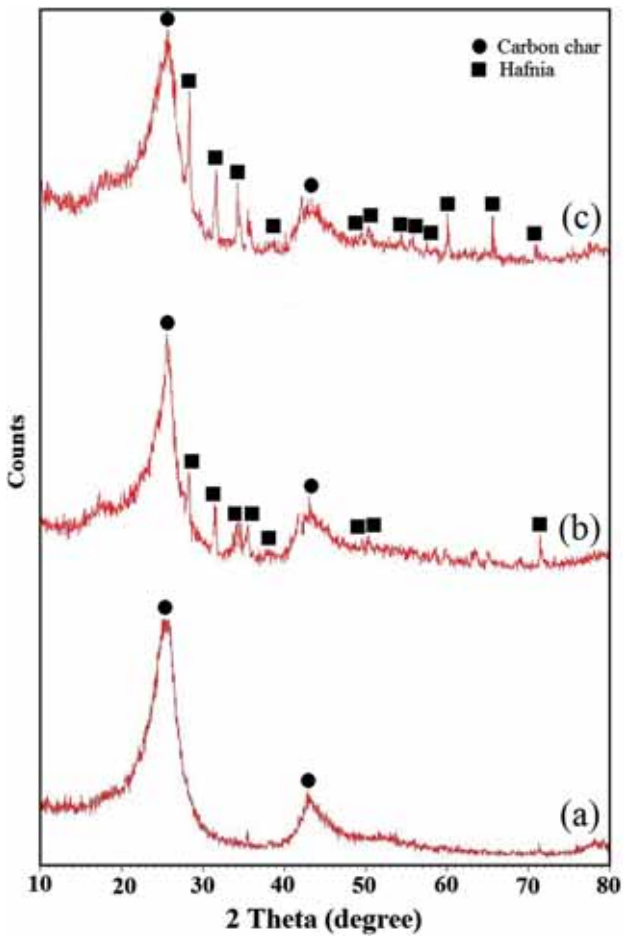

Figure 4. Diffraction pattern of (**a**) pristine and reinforced C–C composites with (**b**) HfB_2 and (**c**) HfB_2/MWCNT after exposure to the flame at 2500°C for 160 s.

were covered by a kind of white solids after ablation [33]. The white solids on the surface of the composites were analysed by XRD, and it turned out to be hafnium dioxide (HfO_2) and amorphous carbon from phenolic by the analysis result shown in figure 4b and c. In the ablating progress, the introduced hafnium diboride nanoparticles were converted into hafnium dioxide. The obtained oxide of HfB_2 has an appropriately high

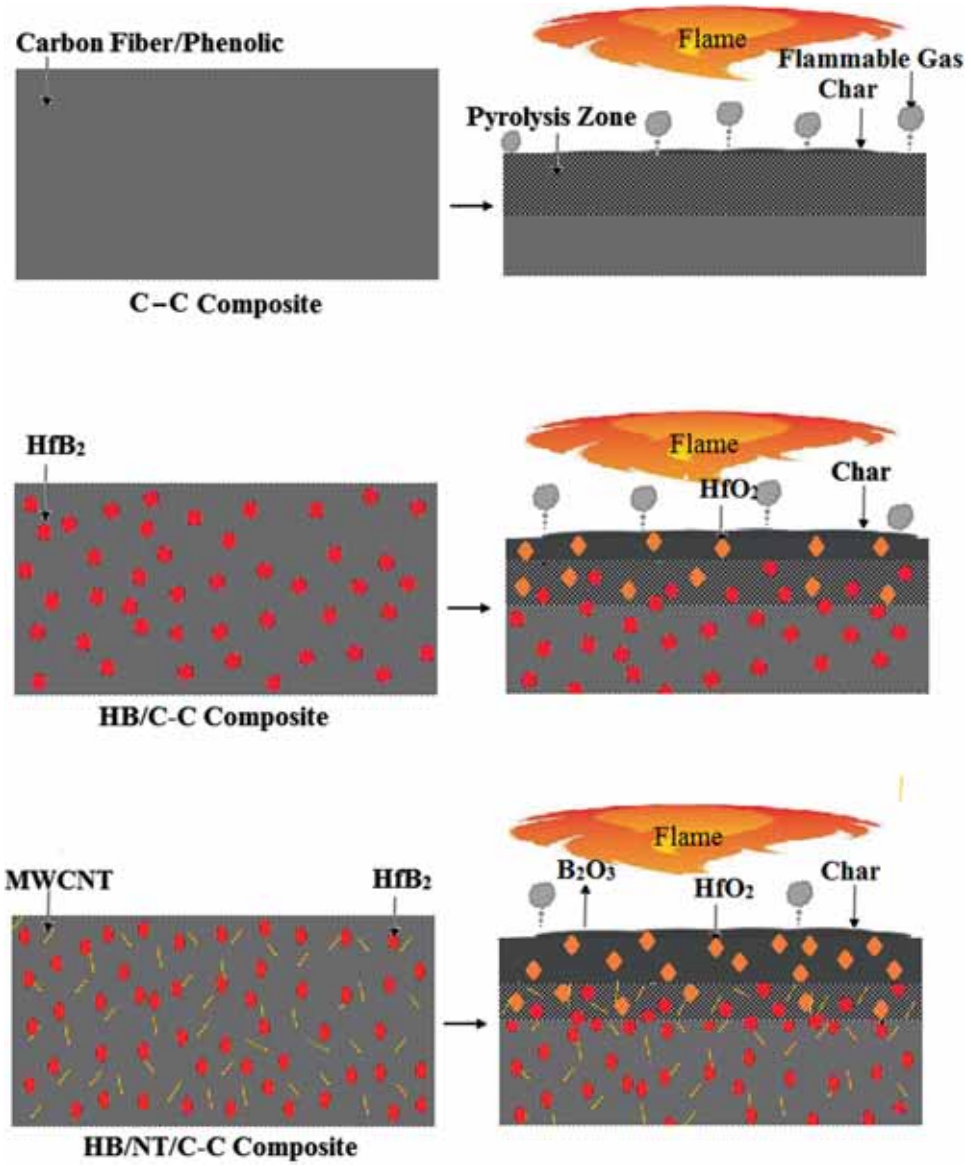

Figure 5. Schematic diagram of the ablation process of (**a**) C–C, (**b**) HB/C–C and (**c**) HB/NT/C–C composites.

melting point (HfO_2: 2750°C) and a relatively low vapour pressure, which acted as an insulating course during ablation [34]. On the surface of HB/NT/C–C, the char network imbues the more decomposition products and creates more char than HB/C–C as shown in figure 3d. Hence, the char layer significantly enhanced the flame retardancy of the composites and scaled down further degradation and reduction in HB/NT/C–C.

The mass and linear ablation rates for pure C–C and two nanocomposites were calculated based on experimental results. For C–C composite, the result of the oxidation surface showed a mechanical scour resulted from blowing the oxyacetylene flame, corresponding to the large rates of mass erosion ($0.025\,g\,s^{-1}$) and linear ablation ($15.6\,\mu m\,s^{-1}$). The more compact and homogeneous oxide scale was formed on two nanocomposites, and no cracks were observed during oxidation or after being cooled down from an elevated temperature. It is clear that with the introduction of 4 wt% HfB_2, the ablation properties of C–C composites were significantly improved. Therefore, the HB/C–C composite achieved both good mass ablation rate and linear ablation rate, which were $0.016\,g\,s^{-1}$ and $7.5\,\mu m\,s^{-1}$, respectively. The mass ablation and linear ablation rates were found to be as low as $0.015\,g\,s^{-1}$ and $1.3\,\mu m\,s^{-1}$, for 1 wt% MWCNT and 4 wt% HfB_2, indicating a lower erosion rate and preserved integrity of the structure. Therefore, rates for HB/NT/C–C nanocomposite were found to be lower than C–C and HB/C–C composites. Significantly, lower rates of linear ablation (91%) and mass erosion (40%) were achieved in the C–C composite

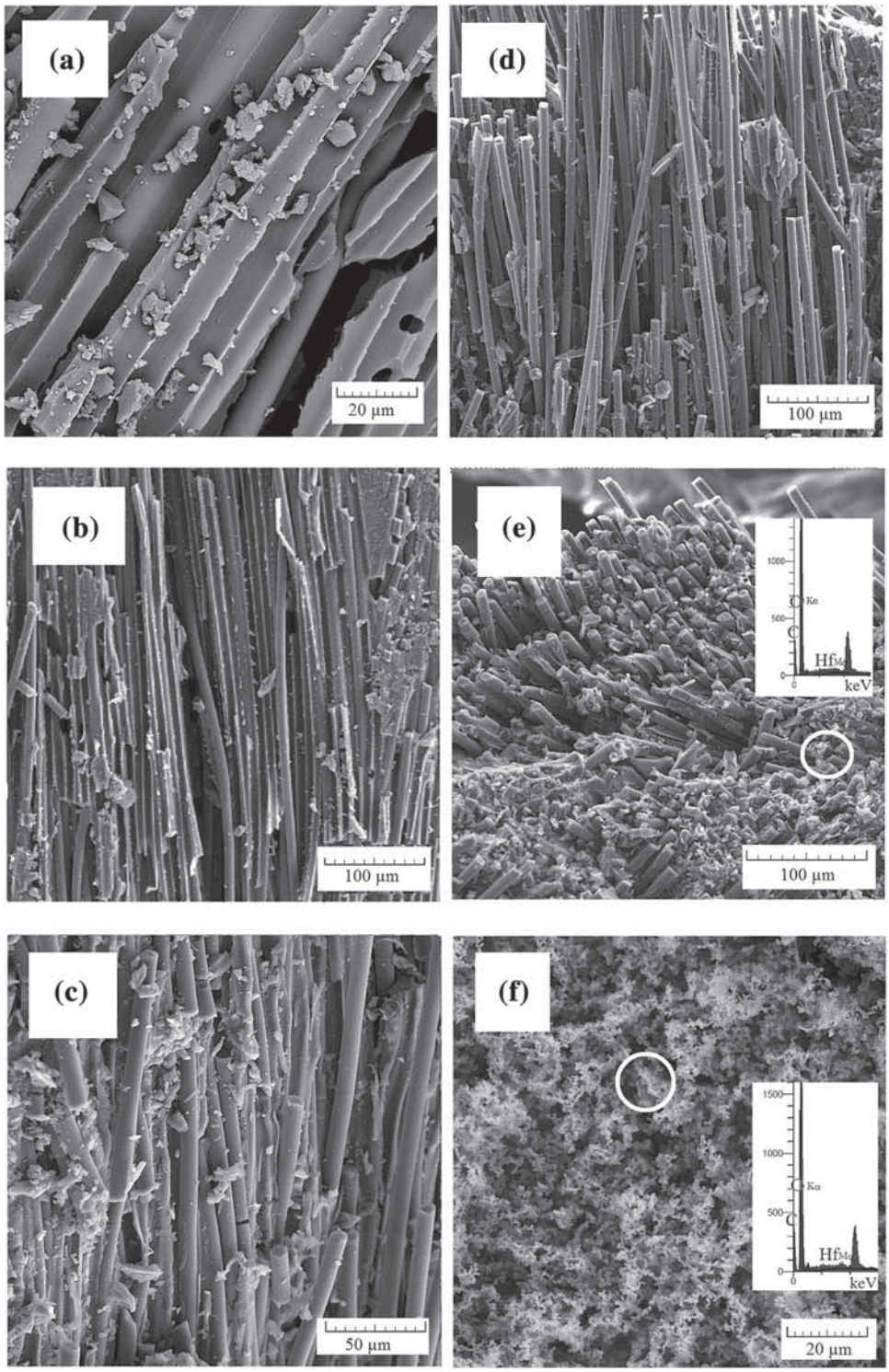

Figure 6. FESEM images of (**a**) C–C, (**b**) HB/C–C and (**c**) HB/NT/C–C composites before the oxyacetylene torch test; and (**d**) C–C, (**e**) HB/C–C and (**f**) HB/NT/C–C after exposure to the flame at 2500°C for 160 s.

with MWCNT and HfB_2 nanoparticles; and linear ablation and mass erosion of HB/C–C were 51 and 36%, respectively. A relatively tough and inorganic char forms during the ablation of these nanocomposites resulting in at least an order-of-magnitude decrease in the mass loss rate relative to the neat polymer [35].

Ablation mechanism of charring ablative composites is assumed to form the porous carbonaceous char layer by

the thermal degradation of the carbon fibre–novolac as the pyrolysis moves into the unablated zone of the virgin section as shown in figure 5. During the ablation test, the outermost layer of the materials (pyrolysing phase) in contact with the outer atmosphere undergoes mass loss and carbonization upon endothermic dissociation of the polymer, producing pyrolysis gases. This heat is dissipated and circulated away from the boundary layer, leading to potent heat shielding. The formed char plays a significant role in the ablation behaviour, because it is capable of absorbing the heat generated during the ablation process [36]. At the end of the pyrolysis process, part of the matrix has turned into a gaseous mixture (pyrolysis gas) and part of it adds to the charred porous material. The pyrolysis gas mass is mostly constituted by CO and H_2 with C_2H_2 becoming important only at higher temperatures [37]. During the decomposition, the ablative composite produces pyrolysis gases in the reaction zone and degrades to a char layer [38]. The presence of the char layer affects the penetration of heat from the surface and produces a steep temperature gradient [39]. The microcracks and pores of the hot char layer allow the gaseous decomposition products such as hydrocarbons and hydrogen to percolate through it by diffusion. The endothermic gases undergo heat exchange with the incoming heat flux and surroundings at the surface of the ablator. The improved oxidation resistance mechanism of the C–C composite with added HfB_2 could be obtained as follows: during the ablation process, combined with the oxidation of HfB_2 and the evolution of volatile products (B_2O_3 and CO), a porous structure of oxide layers was formed. In figure 5, for composite HB/C–C, the occurrence of HfO_2 phase could spread over the oxidation surface, and prevented the inward penetration of O_2, then, provided a better protection on the oxidation layer. Furthermore, it was observed that in the initial stages of pyrolysis, B_2O_3 is obtained [40]. The B_2O_3 glassy phase could fill the voids in the HfO_2 framework below 1200°C and provide the oxidation layer with a moderate strength, preventing it from breaking [41]. When MWCNTs incorporated into the HB/C–C composite, the thermal response of the surface continued with crosslinking reactions, which resulted in the incorporation of the resulting composition into the HfO_2–MWCNT networks [42]. Such a decomposition pathway can be favoured and significantly inhibits the loss of char containing particles. As a result, along with degradation of HfB_2, MWCNT also dissociates and results in the change of the surface structure. Therefore, it can be concluded that the decomposition proceeds with the formation of HfO_2 [43]. Thereafter, heating and formation of HfO_2–MWCNT occur, which is the another important degradation process.

3.5 *Electron microscopy of the nanocomposites*

It can be seen from figure 6a and b that carbon fibres have smooth and clean surfaces, indicating that the interfacial adhesion was relatively weak for C–C and HB/C–C composites. For the HB/NT/C–C composite, a big amount of matrix with MWCNTs was attached onto the fibre surfaces as shown in figure 6c, indicating that the interfacial adhesion was relatively sufficient. At the 1 wt% of MWCNT and 4 wt% of HfB_2, there was a big amount of matrix attached to the fibre surfaces as shown in figure 6c. Figure 6d–f shows the enlargement morphologies of the ablation centre. The axial alignment of the fibres in the C–C composite is perpendicular to the ablation direction of the flame in figure 6d. The HfB_2 in HB/C–C that initially attached to surrounding fibres are all peeled off after the ablation and scour by the flame [44], as illustrated in figure 6e, in this area, the axial fibres are perpendicular to the ablation direction indicating the ablation in this area. The introduced hafnium diboride transported into hafnium dioxide via oxidation reactions, and the hafnium dioxide particles were blown to both sides of the centre by the strong flow. Hence, a few solid particles were formed in this area. Compared with these two composites, HB/NT/C–C had a higher carbon residual value. Figure 6f shows the pursuit for effective ablative composite with a higher char retention property and improved erosion rate for HB/NT/C–C. EDS was performed on the oxide layer of HB/C–C and HB/NT/C–C to examine the amounts of HfB_2. It indicated that the oxide layer contained Hf, O and C.

4. Conclusion

A novel nanocomposite of carbon–novolac reinforced with MWCNT and HfB_2 nanoparticles was prepared and investigated for potential use in ultra-high temperature applications. The high bond dissociation energy of the polymer composite and uniform formation of interconnected nanospheres significantly reduced the flow of oxygen into the virgin material substrate. In addition, at high velocities, the diffusion of the outgoing flux of the endothermic pyrolysis gaseous reaction products through the pores hindered the motion of heat flux, and this led to the considerable diminution of the effect of incoming erosive heat flux. It also ensured enhanced ablation characteristics. Quantifying the ablation characteristic in thickness of the samples occurred during the ablation test, and a reduction of 91% in HB/NT/C–C and of 51% in HB/C–C was noted, advocating the char network modification by HfO_2 and MWCNT. This authenticated the compatibility between the charred surface and nanospheres formed, and hence, HfO_2/MWCNT units also help in maintaining the integrity of the specimen by improving the char retention property, thus further embellishing thermal stability.

References

[1] Bai X, Li F, Li C and Zhang S 2006 *Fiber Reinforced Plastics/Composites* **6** 013

[2] Li H, Yao D, Fu Q, Liu L, Zhang Y, Yao X *et al* 2013 *Carbon* **52** 418

[3] Balaji R, Sasikumar M and Elayaperumal A 2015 *Polym. Degrad. Stab.* **114** 125
[4] Zapata-Solvas E, Jayaseelan D, Brown P and Lee W 2014 *J. Eur. Ceram. Soc.* **34** 3535
[5] Gasch M, Johnson S and Marschall J 2008 *J. Am. Ceram. Soc.* **91** 1423
[6] Wang Y, Li H, Fu Q, Wu H, Yao D and Wei B 2011 *Appl. Surf. Sci.* **257** 4760
[7] Wang Y, Xiong X, Li G, Liu H, Chen Z, Sun W *et al* 2012 *Corros. Sci.* **65** 549
[8] Wang Y, Xiong X, Zhao X, Li G, Chen Z and Sun W 2012 *Corros. Sci.* **61** 156
[9] Yan M, Li H, Fu Q, Xie J, Liu L and Feng B 2014 *Acta Metall. Sin.* **27** 981
[10] Zhang Y, Ren J, Tian S, Li H and Hu Z 2014 *Appl. Surf. Sci.* **311** 208
[11] Paul A, Venugopal S, Binner J, Vaidhyanathan B, Heaton A and Brown P 2013 *J. Eur. Ceram. Soc.* **33** 423
[12] Ren X, Li H, Chu Y, Fu Q and Li K 2015 *Int. J. Appl. Ceram. Technol.* **12** 560
[13] Carney C M, Parthasarathy T A and Cinibulk M K 2013 *Int. J. Appl. Ceram. Technol.* **10** 293
[14] Monteverde F and Bellosi A 2005 *J. Eur. Ceram. Soc.* **25** 1025
[15] Amirsardari Z, Aghdam R M, Salavati-Niasari M and Shakhesi S 2015 *J. Therm. Anal. Calorim.* **120** 1535
[16] Liu L, Li H, Zhang Y, Shi X, Fu Q, Feng W *et al* 2015 *Ceram. Int.* **41** 1823
[17] Lu J, Hao K, Liu L, Li H, Li K, Qu J *et al* 2016 *Corros. Sci.* **103** 1
[18] Amirsardari Z, Aghdam R M, Salavati-Niasari M and Shakhesi S 2015 *Compos. Part B Eng.* **76** 174
[19] Park J, Kwon D, Wang Z, Roh J, Lee W, Park J *et al* 2014 *Compos. Part B Eng.* **67** 22
[20] Wang Z, Kwon D, Gu G, Lee W, Park J, DeVries K *et al* 2014 *Compos. Part B Eng.* **60** 597
[21] Yi X, Feng A, Shao W and Xiao Z 2016 *High Perform. Polym.* **28** 505
[22] Zhang Y F, Zhang J X, Lu Q M and Zhang Q Y 2006 *Mater. Lett.* **60** 2443
[23] Ni D, Zhang G, Kan Y and Wang P 2008 *J. Am. Ceram. Soc.* **91** 2709
[24] Martin-Gallego M, Verdejo R, Lopez-Manchado M A and Sangermano M 2011 *Polymer* **52** 4664
[25] Barun D, Prasad K E, Ramamurty U and Rao C N R 2009 *Nanotechnology* **20** 125705
[26] Shi Y, Feng X, Wang H and Lu X 2008 *Wear* **264** 934
[27] Park J K and Kang T J 2002 *Carbon* **40** 2125
[28] Bessire B K, Lahankar S A and Minton T K 2014 *ACS Appl. Mater. Interf.* **7** 1383
[29] McManus H L and Springer G S 1992 *J. Compos. Mater.* **26** 206
[30] Minus M and Kumar S 2005 *JOM* **57** 52
[31] Gao G, Zhang Z, Li X, Meng Q and Zheng Y 2010 *Polym. Bull.* **64** 607
[32] Chen Y, Chen P, Hong C, Zhang B and Hui D 2013 *Compos. Part B Eng.* **47** 320
[33] Weng L, Zhang X, Han W and Han J 2009 *Int. J. Refract. Metals Hard Mater.* **27** 711
[34] Carney C M, Parthasarathy T A and Cinibulk M K 2011 *J. Am. Ceram. Soc.* **94** 2600
[35] Ho W K, Koo J H and Ezekoye O A 2010 *J. Nanomater.* **2010** 1
[36] Cho D, Lee J and Yoon B 1993 *J. Mater. Sci. Lett.* **12** 1894
[37] Bianchi D, Turchi A, Nasuti F and Onofri M 2013 *J. Propul. Power* **29** 1220
[38] Pope R B and Vojvodich N S 1964 *AIAA J.* **2** 536
[39] Dickey R R, Lundell J H and Wakefield R M 1969 *J. Spacecr. Rockets* **6** 122
[40] Monteverde F 2007 *J. Alloys Compd.* **428** 197
[41] Monteverde F and Bellosi A 2004 *Adv. Eng. Mater.* **6** 331
[42] Song Y I, Yang C M, Kwac L K, Kim H G and Kim Y A 2011 *Appl. Phys. Lett.* **99** 153115
[43] Zhang X, Weng L, Han J, Meng S and Han W 2009 *Int. J. Appl. Ceram. Technol.* **6** 134
[44] Paul A, Binner J, Vaidhyanathan B, Heaton A and Brown P M 2016 *Adv. Appl. Ceram.* **115** 158